Revised Implicit Solvent Model for the Simulation of Surfactants in Aqueous Solutions

Shintaro Morisada, Hiroyuki Shinto,* and Ko Higashitani

Department of Chemical Engineering, Kyoto University, Nishikyo-ku, Kyoto 615-8510, Japan

Received: February 3, 2005; In Final Form: April 18, 2005

The implicit solvent model (ISM) proposed previously for the simulation of surfactant aqueous solutions, in which no water molecules of the solvent are treated explicitly, but the effects are incorporated using the solvent-averaged interactions between the surfactant segments in water at infinite dilution, has been revised to represent the surfactant aggregates more appropriately. In the revised model (ISM-2), the interactions between the hydrophobic sites of the surfactants are varied depending on their surroundings, namely, the local hydrocarbon density. The ISM-2 has been applied to the molecular dynamics simulations of (i) the single *n*-hexane droplets of different sizes in water and (ii) the single micelle composed of 30 *n*-decyltrimethylammonium chloride (C_{10}TAC) cationic surfactants. As a result, it was found that the ISM-2 can mimic the *n*-hexane/water interface and represent the fluidity of the hydrocarbon interior of the surfactant micelle that the original ISM fails to do. The results will be compared to those from experiments and atomistic model simulations.

1. Introduction

Surfactant molecules in solutions assemble spontaneously into aggregates such as spherical and cylindrical micelles, vesicles, and bilayers, depending on their molecular structures as well as the solution conditions. At high surfactant concentrations, the surfactant aggregations develop into long-range ordered phases of liquid crystalline.[1,2] Such surfactants with the self-assembling nature have been used in a wide range of industrial processes as detergents, emulsifiers, dispersants, and lubricants. Recently, the self-assembled structures of surfactants have been utilized as templates for the synthesis of organic and inorganic nanomaterials.[3−7] In these industrial and material processes, it is crucial to understand the relation between the behavior of the surfactant self-assembly and the structures of the surfactants or the solution conditions at the molecular level.

With the help of increasing computational power, computer simulations based on a molecular dynamics (MD) or a Monte Carlo (MC) method have become an important tool in analyzing the microscopic features of matter and materials.[8−10] For studying the molecular-level behavior of surfactants in aqueous solutions, several research groups carried out the MD and MC simulations of surfactant systems.[11−23] However, it is still difficult to simulate the self-assembly of surfactants using the atomistic models because long-time simulations of the large-scale systems are required to examine the surfactant self-assembly.

Let us consider the solutions, in which the number of the solvent molecules is extremely larger than that of the solutes of interest. If the solvent molecules are treated implicitly, then the long-time simulations of the large-scale systems can be realized. Such implicit treatment of the solvent is referred to as an implicit solvent model (ISM),[24] in which the effects of the solvent are incorporated into the interactions between the solutes. When the concentration of the solutes is not very high, the effective interactions between them are represented plausibly by the potential of mean force (PMF), which is the solvent-averaged free energy as a function of the configuration of the solutes and consists of the sum of the *direct* and the *solvent-induced* interactions. Recently, we performed the simulations of cationic surfactants in aqueous solutions using the ISM based on the PMFs and demonstrated that our ISM can capture the characteristics of the surfactants in aqueous solutions,[25] where the interactions between the hydrophobic sites of the surfactants were represented by the PMF for the methane pair in water at infinite dilution. In the strict sense, however, this model is not satisfactory for representation of the surfactant aggregates such as micelles. This is because the solvent-induced interactions between the hydrophobic sites (i.e., the hydrophobic interactions) are negligible in the interior of the micelle, where water molecules hardly exist, and hence only the direct interactions should be considered. The aim of the present study is to improve the ISM of surfactant solutions, which was given in our previous study.[25]

In this paper, the ISM for the simulation of surfactants in aqueous solutions is revised, where the interactions between the hydrophobic sites of the surfactants are varied depending on the hydrocarbon densities around them. To check whether the modified ISM (ISM-2) represents the interactions plausibly, we apply it to the MD simulation of the oil droplets of *n*-hexane in water, where the interfacial tension of the *n*-hexane/water interface is calculated. A single micelle of the surfactants in water is then examined by the MD simulation with the ISM-2, and the simulation results are compared to those from the ISM.

2. Simulation Methods

2.1. Models. We consider *n*-decyltrimethylammonium chloride [$CH_3(CH_2)_9-N(CH_3)_3^+Cl^-$ or C_{10}TAC] and water as a cationic surfactant and a solvent, respectively. To construct the force field of the surfactant molecule using the PMFs, we employed the following technique. The hydrophilic and the hydrophobic groups of the surfactant were approximated by a tetramethylammonium ion [$(CH_3)_4N^+$ or TMA^+] and a chain of methane molecules (CH_4 or Me), respectively. The PMFs

* Corresponding author. Tel: +81-75-383-2672. Fax: +81-75-383-2652. E-mail: shinto@cheme.kyoto-u.ac.jp.

10.1021/jp050600q CCC: $30.25
Published on Web 05/20/2005

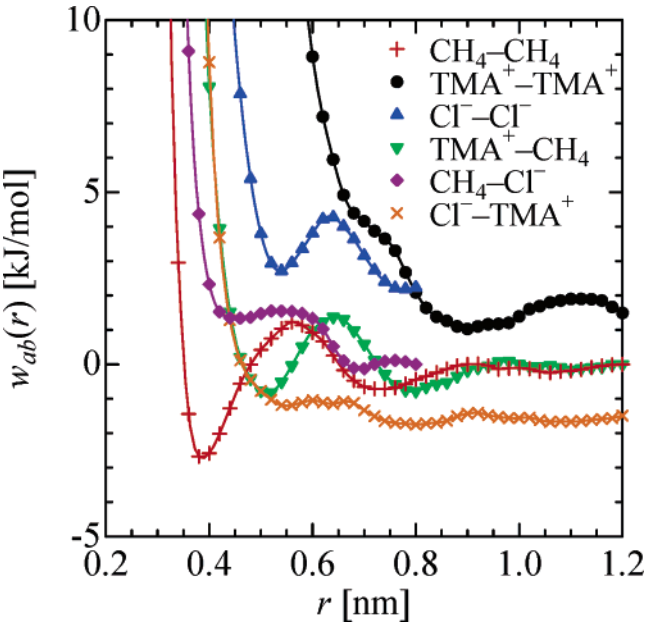

Figure 1. Potentials of mean force for solute pairs in ambient water at infinite dilution. The solid lines are the guides for the eyes.

TABLE 1: Molecular Geometry of Surfactant ($t_{10}h^+$) and *n*-Hexane (t_6)

	bond length (nm)	bond angle (deg)
t−t	0.153	
t−h$^+$	0.280	
t−t−t		109.5
t−t−h$^+$		126.4

for six different binary combinations with Me, TMA^+, and Cl^- in ambient water at infinite dilution were computed as a function of the intersolute distance using the atomistic model MD simulations,[26] where the water molecules as well as the solutes were treated explicitly. Figure 1 displays the resultant PMFs $w_{ab}(r)$. The surfactant of $CH_3(CH_2)_9-N(CH_3)_3^+Cl^-$ was mimicked as $(Me)_{10}-TMA^+Cl^-$, that is, $t_{10}h^+Cl^-$, where t and h^+ denote the hydrophobic and the hydrophilic sites, respectively. Likewise, an *n*-hexane molecule of $CH_3(CH_2)_4CH_3$ was modeled as t_6.

2.1.1. Implicit Solvent Model (ISM). The intermolecular potentials for $t_{10}h^+-t_{10}h^+$, $t_{10}h^+-Cl^-$, and Cl^--Cl^- interactions as well as for t_6-t_6 interaction were given by assuming the site−site pair additivity of the PMFs. The PMFs for separations beyond the range of the computed PMFs (i.e., $r > 0.8$ or 1.2 nm) were given by

$$w_{ab}(r) = \frac{1}{4\pi\epsilon_r\epsilon_0}\frac{Q_aQ_b}{r} \tag{1}$$

where Q_a is the point charge of site a, ϵ_0 is the permittivity of the vacuum, and ϵ_r is the relative permittivity of water; the experimental value of $\epsilon_r = 77.6$ at $T = 300$ K was used.[27]

As for the intramolecular interactions of the t_6 oil and the $t_{10}h^+$ surfactant, only the PMFs between the sites separated by at least four bonds were included. The bond lengths and the bond angles were fixed at constant values, as listed in Table 1. The torsional potential proposed by Ryckaert and Bellemans[28] was used for t−t−t−t and t−t−t−h$^+$

$$u_{\text{torsion}}(\phi) = \sum_{n=0}^{5} k_n \cos^n\phi \tag{2a}$$

$$\left.\begin{aligned} k_0 &= +1.541 \times 10^{-20}\ \text{J} \\ k_1 &= +2.019 \times 10^{-20}\ \text{J} \\ k_2 &= -2.179 \times 10^{-20}\ \text{J} \\ k_3 &= -0.508 \times 10^{-20}\ \text{J} \\ k_4 &= +4.357 \times 10^{-20}\ \text{J} \\ k_5 &= -5.230 \times 10^{-20}\ \text{J} \end{aligned}\right\} \tag{2b}$$

where ϕ is the dihedral angle and $\phi = 0$ corresponds to the trans conformation.

2.1.2. Revised Implicit Solvent Model (ISM-2). Henceforth, we describe how the ISM mentioned above was revised. The interaction force between the hydrophobic sites, $f_{tt}(r)$, was represented by the PMF and the Lennard-Jones (LJ) terms

$$f_{tt}(r) = -(1-\alpha_{ia,jb})\frac{dw_{MeMe}(r)}{dr} - \alpha_{ia,jb}\frac{du_{LJ}(r)}{dr} \tag{3a}$$

$$u_{LJ}(r) = 4\epsilon\left[\left(\frac{\sigma}{r}\right)^{12} - \left(\frac{\sigma}{r}\right)^{6}\right] \tag{3b}$$

where $w_{MeMe}(r)$ is the PMF for the CH_4-CH_4 pair (see Figure 1), $\epsilon = 0.994 \times 10^{-21}$ J, and $\sigma = 0.3923$ nm; the latter two are the energy and the size parameters of the LJ potential for *n*-alkane, respectively.[28] As described below, the distribution parameter, $\alpha_{ia,jb}$, is allowed to vary from 0 to 1, depending on the local packing ratio of the hydrocarbon sites around sites a and b of interest.

To define the local packing ratio of the hydrocarbon sites around site a on molecule i, Γ_{ia}, we regarded every hydrophobic site as a sphere of radius $\sigma/2$ and then computed the portion that the spherical shell of inner radius $\sigma/2$ and outer radius σ around site a cuts out from the spheres of all of the other sites, as illustrated in Figure 2. The spherical shell around site a on molecule i cuts out from the sphere of site b on molecule j, the shaded portion, whose volume, V_{ia}^{jb}, is

$$V_{ia}^{jb}(r_{ab}) = \begin{cases} (13\pi/192)\sigma^3, & r_{ab} < \sigma \\ \dfrac{\pi\sigma^4}{12r_{ab}}\left(\dfrac{r_{ab}}{\sigma}-\dfrac{3}{2}\right)^2\left[\left(\dfrac{r_{ab}}{\sigma}+\dfrac{3}{2}\right)^2-3\right], & \sigma \le r_{ab} \le 3\sigma/2 \\ 0, & r_{ab} > 3\sigma/2 \end{cases} \tag{4}$$

Notice that $V_{ia}^{jb} = V_{jb}^{ia}$. The other shaded portion is cut out from the spheres of the neighboring sites ($=a \pm 1$, $a \pm 2$, $a \pm 3$) and then excluded from the spheres of the sites $a \pm 4$; this volume is denoted by V_{ia}. Consequently, the local packing ratio, Γ_{ia}, is defined as

$$\Gamma_{ia} = \frac{1}{V_{cp}}\left[V_{ia} + \sum_{b\le a-4, b\ge a+4}\beta_b V_{ia}^{ib}(r_{ab}) + \sum_{j\neq i}\sum_{b\in j}\beta_b V_{ia}^{jb}(r_{ab})\right] \tag{5}$$

where the first, second, and third terms in the brackets correspond to the contributions from the intramolecular neighboring sites, the other intramolecular sites, and all of the sites of the other molecules, respectively. In eq 5, $V_{cp} \equiv V_{id}^{jb}(\sigma) \times 12 = (13\pi/16)\sigma^3$ is the closest packing volume for the nonbonded identical spheres of radius $\sigma/2$ and β_b is a factor to avoid overestimating the net volume occupied by molecule j (e.g., the simple summation of V_{id}^{jb} over site b on molecule j causes overestimation of the volume of the overlapping space

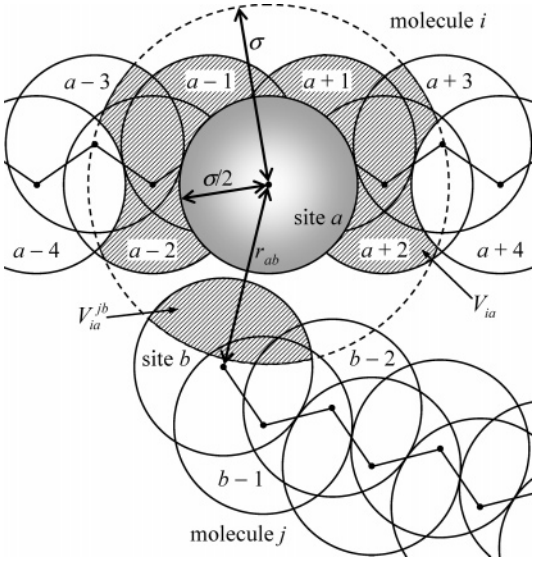

Figure 2. Illustration of hydrophobic chains of two molecules. The spherical shell of inner radius $\sigma/2$ and outer radius σ around site a on molecule i cuts out from the sphere of site b on molecule j, the shaded portion, whose volume is indicated by V_{ia}^{jb}. The other shaded portion is cut out from the spheres of the neighboring sites ($=a \pm 1$, $a \pm 2$, $a \pm 3$) and then excluded from the spheres of sites $a \pm 4$; this volume is denoted by V_{ia}.

TABLE 2: Parameters of Eq 5 for *n*-Hexane (t_6)

	V_{ia}/V_{cp}	β_b
t1, t6	0.20	0.75
t2, t5	0.31	0.59
t3, t4	0.43	0.53

TABLE 3: Parameters of Eq 5 for Surfactant ($t_{10}h^+$)

	V_{ia}/V_{cp}	β_b
t1	0.61	0.53
t2	0.51	0.54
t3	0.43	0.53
t4, t5, t6	0.40	0.53
t7	0.42	0.53
t8	0.41	0.53
t9	0.31	0.59
t10	0.20	0.75

between the spherical shell of site a on molecule i and a chain of the spheres on molecule j). The distribution parameter, $\alpha_{ia,jb}$, is given as a function of the local packing ratio around sites a and b of interest, $\Gamma_{ia,jb}$

$$\alpha_{ia,jb} = 0.5 + 0.5 \tanh\left[\frac{\Gamma_{ia,jb} - 0.5}{0.135}\right] \tag{6a}$$

$$\Gamma_{ia,jb} = \max(\Gamma_{ia}, \Gamma_{jb}) - \frac{V_{ia}^{jb}(r_{ab})}{V_{cp}} \tag{6b}$$

In the present model, V_{ia} and β_b were chosen as the constant values depending on the sites of the t_6 oil and the $t_{10}h^+$ surfactant, the all-trans configuration of which was assumed for the sake of convenience. The values of parameters V_{ia} and β_b are listed in Tables 2 and 3 for t_6 and $t_{10}h^+$, respectively; the hydrophobic sites of t_6 are numbered 1, ···, 6 from the end t to the other end t, whereas those of $t_{10}h^+$ are numbered 1, ···, 10 from the t next to h^+ to the end t. It should be noted that the aforementioned scheme for calculation of the solvent-induced interaction between the hydrophobic sites using the local packing fraction is analogous to the method of ref 29, where the drag force acting on a colloidal sphere partly surrounded by other spheres in flow fields is calculated using the local void fraction.

TABLE 4: Simulation Systems

system	number of solutes N $t_{10}h^+$	Cl^-	t_6	side length L (nm)	model
A.1			800	50	ISM-2
A.2			1500	50	ISM-2
A.3			2200	50	ISM-2
A.4			3000	50	ISM-2
A.5			5000	50	ISM-2
B.1	30	30		7.927	ISM
B.2	30	30		7.927	ISM-2

2.2. Simulation Details. The systems simulated are summarized in Table 4: (A) single oil droplets composed of different numbers of the *n*-hexane t_6 molecules in water using the ISM-2, where the interfacial tension of the *n*-hexane/water interface was estimated to justify the model; (B) single micelles composed of 30 $t_{10}h^+Cl^-$ surfactants, using both the ISM and the ISM-2. A cubic box with 3D periodicity was employed, which included the finite number of the solutes, N, and had the side length, L, as in Table 4. The equations of motion for all of the interaction sites were integrated by the leapfrog algorithm with the time steps of $\Delta t = 0.001$ ps for system A and $\Delta t = 0.005$ ps for system B. The bond lengths and angles of the t_6 and the $t_{10}h^+$ molecules were fixed by the SHAKE method.[9] The temperature of the systems was kept at $T = 300$ K using the Nosé−Hoover thermostat[9] with a time constant of $\tau_T = 1$ ps. The Coulomb contributions of eq 1 to the PMF were handled by the Ewald summation,[9] whereas the rest of the contributions were considered only within the range of the computed PMFs (i.e., $r \leq 0.8$ or 1.2 nm). In eqs 4−6, the local packing ratio of each hydrocarbon site, Γ_{ia}, was calculated at every time step to update all of the distribution parameters, $\alpha_{ia,jb}$, which were used in eq 3.

2.2.1. Oil Droplets in Water (System A). Single droplets composed of 800, 1500, 2200, 3000, and 5000 t_6 molecules in water were simulated. First of all, the bulk liquid composed of these numbers of *n*-hexane molecules was prepared by the ordinary MD simulation, following Ryckaert and Bellemans,[28] where eq 3 with $\alpha_{ia,jb} \equiv 1$ was employed for all of the nonbonded interactions and the side length of the simulation box was chosen to give the experimental value of the density, 0.66 g cm^{-3}.[30] Using the final configuration, the cubic liquid of *n*-hexane was placed at the center of the larger box of $L = 50$ nm, as shown in part a of Figure 3. Then, the single oil droplet of the t_6 molecules in water was simulated for 300 ps after 100-ps equilibration, using the ISM-2, where the configuration was stored every 0.05 ps for the subsequent analysis.

2.2.2. Surfactant Micelles in Water (System B). Single micelles composed of 30 $t_{10}h^+Cl^-$ surfactants in water were simulated using both the ISM (system B.1) and the ISM-2 (system B.2). It is noted that the average size of the aggregates, N_{av}, for C_{10}TAC is estimated as $N_{av} = 30$, according to an extrapolation of the experimental results for C_nTAC: $N_{av} = 44$, 62, and 84 for $n = 12$,[31] 14,[32] and 16,[33] respectively. The concentration of the surfactants was set at $C_{surf} = 0.1$ M, which is higher than the critical micelle concentration (cmc) of C_{10}TAC in ambient water, 0.05−0.065 M.[34,35] The initial configuration of a micelle was prepared following section 2.4.2 of ref 25, where the time was set at $t = 0$ (see Figure 7), and the system was allowed to evolve over 10 ns. During the 10-ns simulation, the configuration was stored every 0.1 ps for the subsequent analysis.

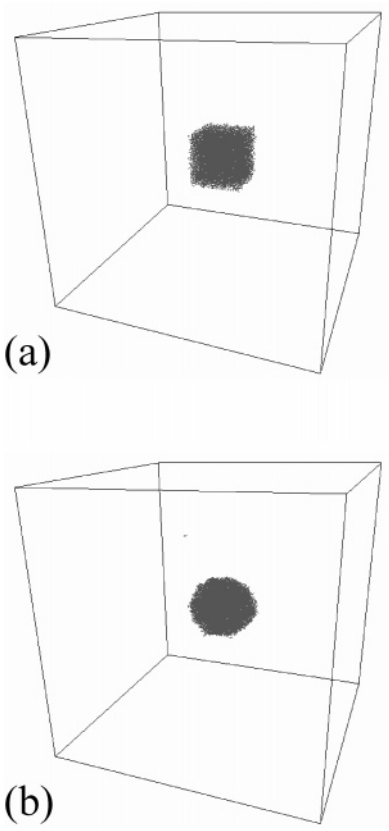

Figure 3. Snapshots of an oil droplet of 5000 t_6 molecules in water (system A.5): (a) the initial configuration; (b) the final configuration. Gray dots denote hydrophobic sites, t. The simulation cell is depicted by the lines.

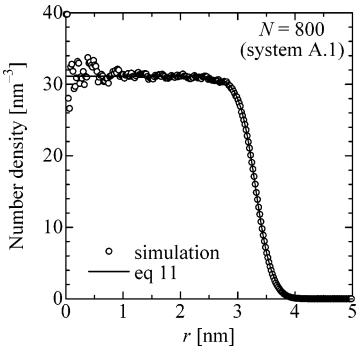

Figure 4. Number density of hydrophobic sites for an oil droplet of 800 t_6 molecules in water (system A.1), as a function of the distance from the center of mass of the droplet. The line represents a fit of eq 11 with $\rho_0 = 31.1$ nm^{-3}, $\rho_\infty = 0$, $R = 3.31$ nm, and $D = 0.29$ nm.

2.3. Calculation of Pressure. To obtain the pressure inside the oil droplet in water, we calculated the normal component of the Irving−Kirkwood pressure tensor[36] following Thompson et al.,[37] who simulated the liquid droplets of LJ particles in the vapor. The normal component of the pressure tensor for the droplet of radius R, p_N, is a function of the distance from the center of mass of the droplet, r, and is represented by the sum of the kinetic and the configurational contributions, p_K and p_U

$$p_N(R; r) = p_K(R; r) + p_U(R; r) \tag{7}$$

The kinetic contribution is given by

$$p_K(R; r) = k_B T \rho(R; r) \tag{8}$$

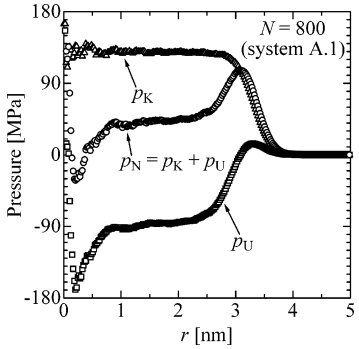

Figure 5. Normal component of the pressure tensor p_N (circles), kinetic contribution p_K (triangles), and configurational contribution p_U (squares) for an oil droplet of 800 t_6 molecules in water (system A.1), as a function of the distance from the center of mass of the droplet. See also section 2.3.

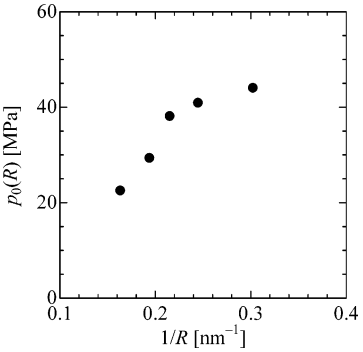

Figure 6. Pressure inside an oil droplet of t_6 molecules in water (system A) as a function of the inverse number of the droplet radius $^1/_R$.

where k_B is the Boltzmann constant and $\rho(R; r)$ is the number density of the hydrophobic sites at r. The configurational contribution is given by

$$p_U(R; r) = \frac{1}{4\pi r^2}\left\langle \sum_k f_k \right\rangle \tag{9}$$

where k represents one of all of the pair forces acting across the spherical surface of radius r, f_k is the normal component of the force between sites a and b, and $\langle \cdots \rangle$ denotes the ensemble average of the function enclosed. Note that f_k is positive and negative for repulsive and attractive forces, respectively. The force, f_k, is represented by

$$f_k = \frac{r_{ab}}{2r}\left[\left(\frac{r_a^2 - r_b^2}{r_{ab}^2}\right)^2 - 2\left(\frac{r_a^2 + r_b^2}{r_{ab}^2}\right) + \frac{4r^2}{r_{ab}^2} + 1\right]^{1/2} f_{ab}(r_{ab}) \tag{10}$$

where r_a is the distance between site a and the center of mass of the droplet and r_{ab} and $f_{ab}(r_{ab})$ are the distance and the force between sites a and b, respectively. Note that $f_{ab}(r_{ab})$ includes the forces for the bond and the angle constraints by the SHAKE method.

3. Results and Discussion

In the following two subsections, we investigate the single oil droplets of *n*-hexane in water (system A) and the single micelles of 30 C_{10}TAC surfactants in water (system B) using MD simulations with the ISM family based on the PMFs.

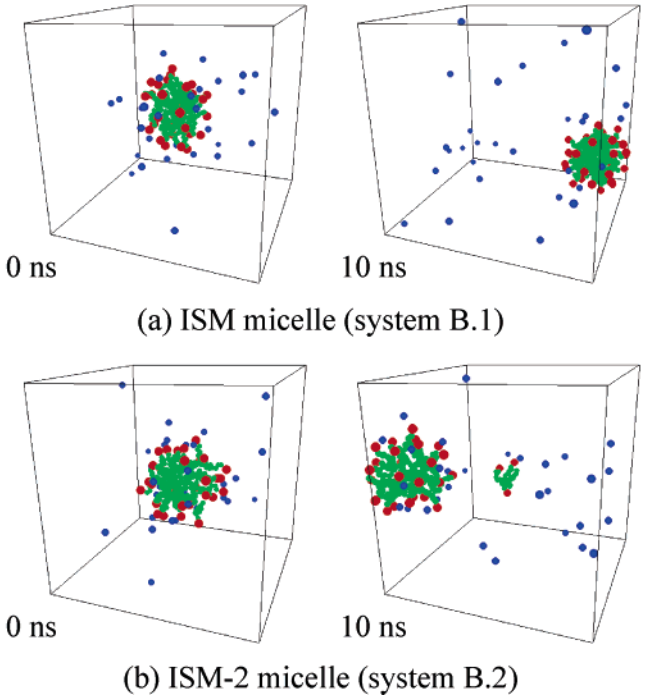

Figure 7. Snapshots of a micelle of 30 $t_{10}h^+Cl^-$ surfactants in water at $C_{surf} = 0.1$ M (system B) at time $t = 0$ and 10 ns: (a) the ISM micelle; (b) the ISM-2 micelle. Green, red, and blue spheres denote t, h^+, and Cl^-, respectively. The simulation cell is depicted by the lines.

3.1. Oil Droplets in Water. Part b of Figure 3 displays the final snapshot of the droplet of 5000 t_6 molecules in *implicit* water (system A.5), where no water molecules are considered explicitly but the effects are incorporated into the ISM-2. The droplet remains aggregated to exhibit a nearly spherical shape, although some oil molecules are leaving the droplet to dissolve in implicit water. Similar behavior was observed for the droplets of the other sizes (systems A.1−A.4).

3.1.1. Density Profiles. The number density of the hydrophobic sites for the droplet of $N = 800$ (system A.1) is plotted in Figure 4, as a function of the distance from the center of mass of the droplet, r. The density profile at the interface is usually described by

$$\rho(R; r) = \frac{\rho_0 + \rho_\infty}{2} - \frac{\rho_0 - \rho_\infty}{2} \tanh\left[\frac{r - R}{D}\right] \qquad (11)$$

where ρ_0 and ρ_∞ denote the densities of the hydrophobic sites inside and outside the droplet, respectively, and D is a measure of the thickness of the interface; we set $\rho_\infty \equiv 0$ in the present study because the number of the dissolved oil molecules is negligible. The fit of eq 11 to the simulation data is also shown in Figure 4, where $\rho_0 = 31.1$ nm^{-3}, $R = 3.31$ nm, and $D = 0.29$ nm. Similar results, $\rho_0 \approx 31$ nm^{-3} and $D \approx 0.3$ nm, were obtained for systems A.2−A.5; the values of R are 4.09, 4.65, 5.16, and 6.13 nm, respectively. These results for the droplets of the t_6 molecules agree with the experimental values of the liquid *n*-hexane density, 28.3 nm^{-3} (=0.66 g cm^{-3}),[30] and the *n*-hexane/water interfacial thickness, 0.4 nm,[38] which is equivalent to $D = 0.4$ nm/1.0986 = 0.36 nm after consideration of the difference between the hyperbolic tangent function of eq 11 and the error function in ref 38.[39]

3.1.2. Pressure Profiles. The pressure profile for the droplet of $N = 800$ is shown in Figure 5. The kinetic contribution, p_K, is positive in the interior of the droplet (i.e., $r < 4.0$ nm), which is a natural consequence of eq 8 and Figure 4. In contrast, the configurational contribution, p_U, is negative in the range of $r <$ 3.0 nm. In the droplet core, the steep reduction of p_U is probably a computational artifact of eq 9 because the ensemble average of the pair forces across the spherical surface of a radius of interest was even poorer with decreasing the radius. It should be noted that the positive values of p_U at $r = 3.0-4.0$ nm could be an artifact caused by the implicit treatment of water molecules. The profile of the net pressure, p_N, at $r = 1.0-2.2$ nm exhibits a nearly constant value of ≈45 MPa, which is considered to be a representative value of the pressures inside the droplet, p_0. Similar profiles were observed in the atomistic model MD simulations of the droplets in the vapor especially for nonpolar LJ particles[40] and for the polar molecules of water[41] and methanol.[42]

3.1.3. Oil/Water Interfacial Tension. The pressure inside the droplet of radius R is defined as $p_0(R) \equiv p_N(R; r = R/2)$ in the present study, and $p_0(R)$ is plotted in Figure 6 as a function of $1/R$. Although the internal pressure, $p_0(R)$, decreases with decreasing $1/R$ as a whole, it greatly decreases for the larger droplets of $N \geq 2200$. For the macroscopic droplets, the relationship between the pressure difference, $p_0(R) - p_\infty$, and the droplet radius, R, is described by the Laplace equation

$$p_0(R) - p_\infty = \frac{2\gamma}{R} \qquad (12)$$

where γ is the interfacial tension. Here, p_∞ is the pressure outside the droplet and can be considered as a constant value regardless of R. We then roughly estimated γ by fitting eq 12 to the simulation data for $N \geq 2200$ in Figure 6, and found the value of $\gamma = 148$ mN/m, which is of the same order as the experimental value of the interfacial tension for a *n*-hexane/water interface, 50.1−51.3 mN/m.[38,43] One may think that eq 12 is not applicable to these small droplets of about 5−6 nm radii because the interfacial tension does depend on the curvature of the interface, that is, the droplet size. However, Nijmeijer et al.[44] obtained the physically reasonable value of the liquid−vapor interfacial tension for the LJ particles of diameter σ_{LJ} after applying eq 12 to the droplets of about $7-13\sigma_{LJ}$ radii, which correspond to about 4−8 nm radii for the droplets of *n*-hexane with $\sigma_{LJ} = 0.5949$ nm.[45] This indicates that the ISM-2 can represent, at least semiquantitatively, the interactions between the hydrophobic sites at the oil/water interface as well as in the bulk liquids of oil and water.

3.2. Surfactant Micelles in Water. Figure 7 displays the snapshots of a micelle of 30 $t_{10}h^+Cl^-$ surfactants simulated by the ISM (system B.1) and the ISM-2 (system B.2). For the ISM micelle, all of the 30 surfactants remained aggregated during $t = 0-10$ ns, as in part a of Figure 7. For the ISM-2 micelle, a few surfactants repeatedly dissociated from and associated with the micelle for $t = 0-10$ ns and the micelle at $t = 10$ ns was composed of 28 surfactants, as in part b of Figure 7. The ISM-2 micelle seems to be soft and enlarged a bit, compared to the ISM micelle.

3.2.1. Structure of Micelles. To investigate the structure of the micelle, we calculated the number densities of t sites, h^+ sites, and Cl^- counterions as a function of the distance from the center of mass of the micelle, r, using the configurations for $t = 8-10$ ns; hereafter, a surfactant is considered to belong to the micelle, when the minimum site-to-site separation between the tail of the surfactant and those of the surfactants in the micelle is less than 0.48 nm, at which the CH_4-CH_4 PMF equals zero, as in Figure 1. The resultant density profiles are shown in Figure 8. For the ISM micelle, the t sites form the hydrocarbon interior of the micelle at $r < 1.4$ nm, whereas the h^+ sites exist

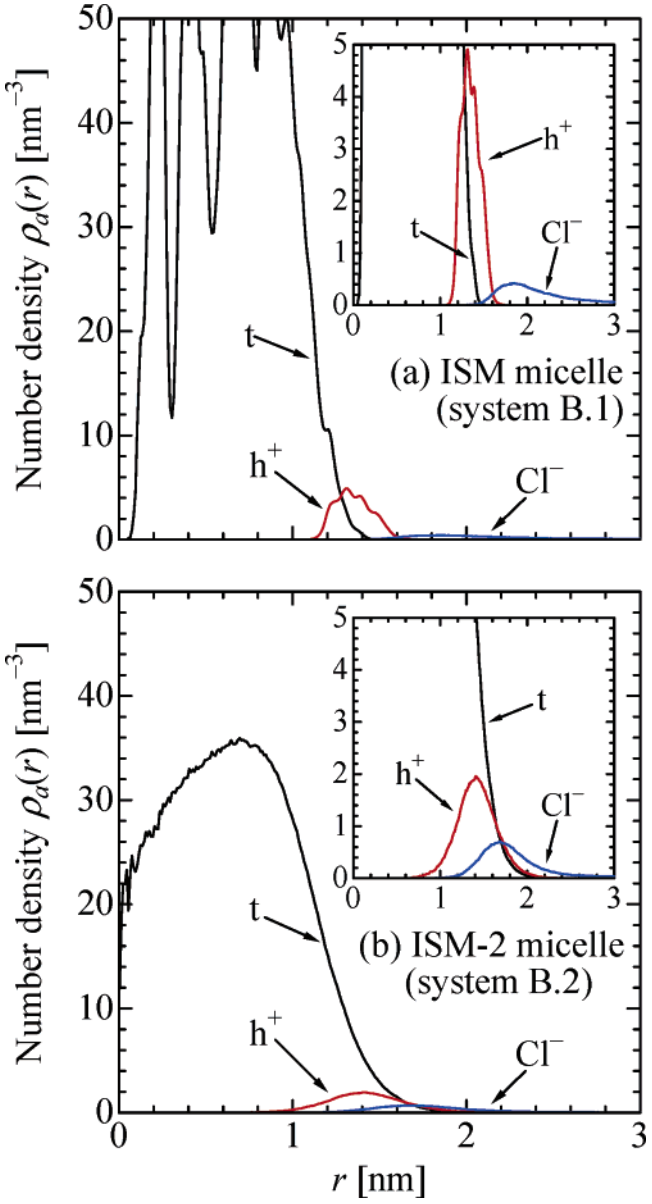

Figure 8. Number densities of t, h^+, and Cl^- for a micelle of 30 $t_{10}h^+Cl^-$ surfactants in water (system B), as a function of the distance from the center of mass of the micelle: (a) the ISM micelle; (b) the ISM-2 micelle. Each density is the result averaged over 20 000 configurations during the last 2 ns of the 10-ns simulation. The insets focus on the densities of the charged sites.

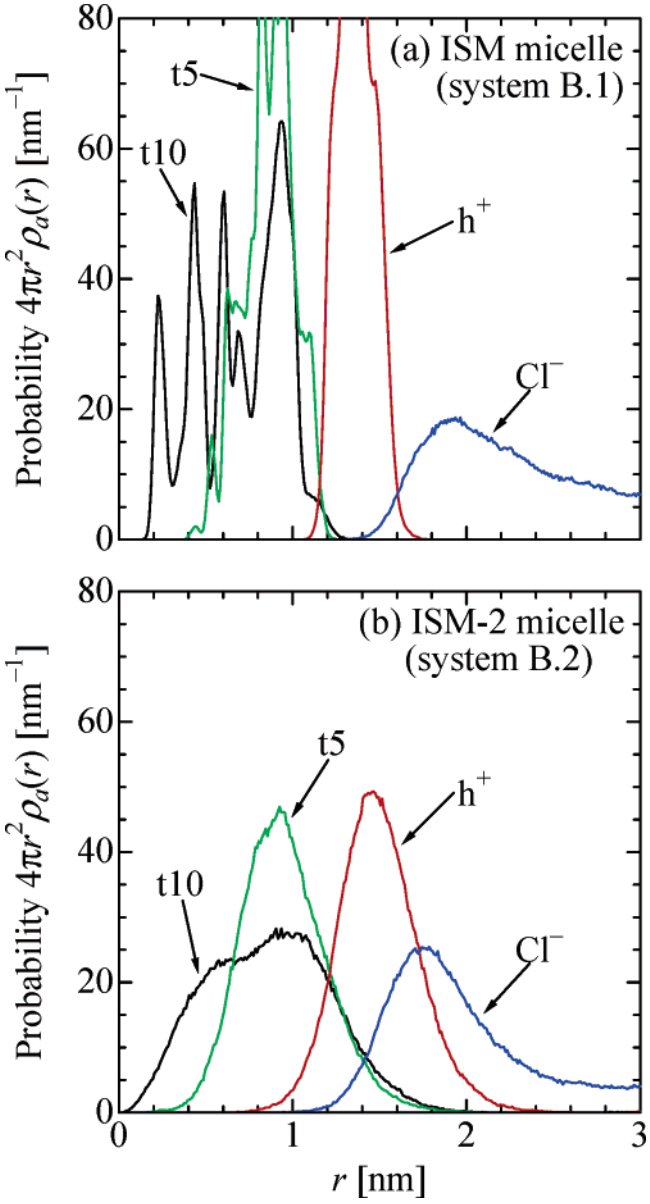

Figure 9. Probabilities of t10, t5, h^+, and Cl^- for a micelle of 30 $t_{10}h^+Cl^-$ surfactants in water (system B), as a function of the distance from the center of mass of the micelle: (a) the ISM micelle; (b) the ISM-2 micelle. Each probability is the result averaged over 20 000 configurations during the last 2 ns of the 10-ns simulation.

at the surface of the hydrocarbon core, as shown in part a of Figure 8. The Cl^- counterions are located outside the micelle and favorably reside near the h^+ sites because of the attractive electrostatic interaction. Similar profiles are obtained for the ISM-2 micelle as in part b of Figure 8, although they have broader peaks. In particular, although the profile of the t sites for the ISM micelle has several sharp peaks, the ISM-2 micelle exhibits a smooth profile; the latter coincides with the result of the atomistic model MD study, where a micelle of 30 C_{10}TAC surfactants was simulated in 2166 water molecules at 0.67 M for 0.215 ns.[46]

The probability distributions of every t sites (=t1, ···, t10), h^+ sites, and Cl^- counterions were calculated as a function of r to obtain further information on the inner structure of the micelle, and the results are shown in Figure 9. For the ISM micelle, the probability distributions of the t10 and t5 sites, as well as those of the other t sites (data not shown), have several peaks as in part a of Figure 9, similar to the density profile of the t sites shown in part a of Figure 8. These results indicate that the hydrocarbon interior of the ISM micelle was solid-like. However, the nuclear magnetic resonance (NMR) measurements demonstrated that the micelles have a liquid-like interior.[47] Thus, the ISM fails to represent the liquid-like hydrocarbon interior of a micelle; this deficiency is caused by rude modeling of the t−t interaction, which is simply given by the CH_4−CH_4 PMF regardless of the surroundings of the t sites.

In contrast, the probabilities of the t10 and t5 sites of the ISM-2 micelle exhibit smooth distributions with a broad peak, as in part b of Figure 9, and agree very well with those in the atomistic model MD study.[46] The results shown in part b of Figures 8 and 9 suggest that the ISM-2 succeeds in capturing the fluidity of the hydrocarbon interior of a micelle, which is indicated by the NMR study.[47]

3.2.2. Shape and Stability of Micelles. The principal moments of inertia of the micelle, I_1, I_2, and I_3 ($I_1 \geq I_2 \geq I_3$), were

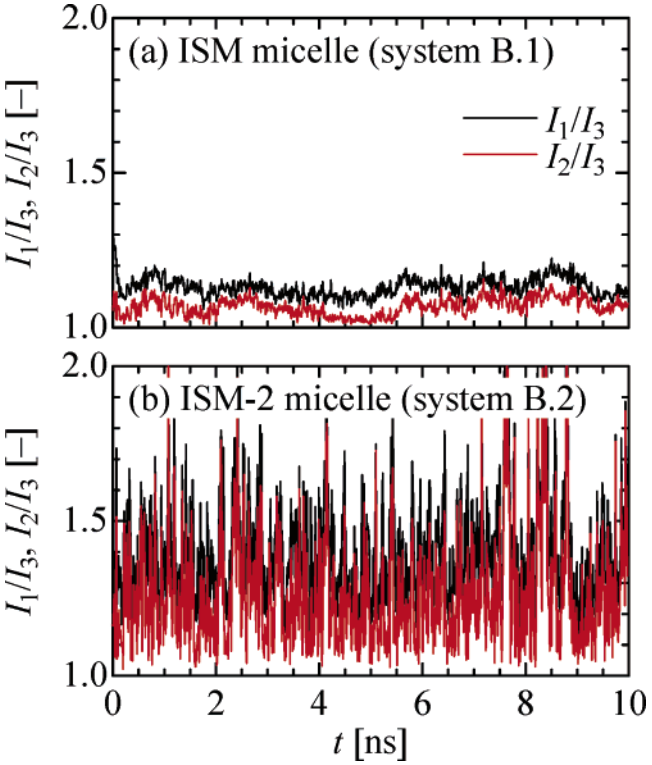

Figure 10. Values of I_1/I_3 (black lines) and I_2/I_3 (red lines) for a micelle of 30 $t_{10}h^+Cl^-$ surfactants in water (system B) as a function of time, t: (a) the ISM micelle; (b) the ISM-2 micelle. The principal moments of inertia of the micelle are represented by I_1, I_2, and I_3, where $I_1 \geq I_2 \geq I_3$. Each plot is the result averaged over 2 ps.

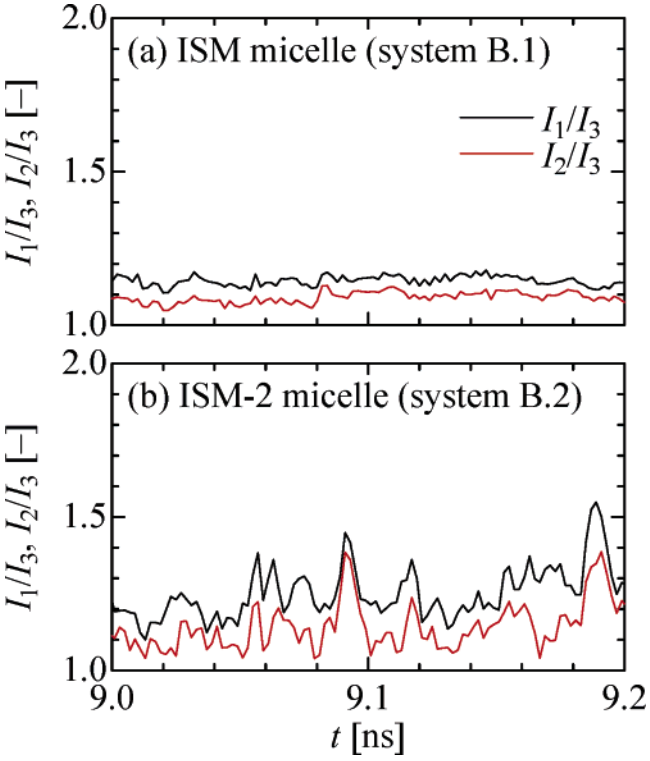

Figure 11. Close-up of Figure 10 within a short period of $t = 9.0-9.2$ ns.

calculated as a function of time, t, to obtain more detailed information on the shape and stability of the micelle. Figure 10 displays the values of I_1/I_3 and I_2/I_3 as a function of time, t, where each plot is the result averaged over 2 ps. The values of I_1/I_3 and I_2/I_3 for the ISM micelle are close to unity (i.e., $I_1 \approx I_2 \approx I_3$), whereas those for the ISM-2 micelle are larger than unity. These results indicate that the ISM micelle is nearly spherical, whereas the ISM-2 micelle has an ellipsoidal shape.

Moreover, I_1/I_3 and I_2/I_3 of the ISM-2 micelle fluctuate considerably compared to those of the ISM micelle, suggesting that the ISM-2 micelle is more fluid and less stable than the ISM micelle. This result is consistent with the snapshots (Figure 7), the density profiles (Figure 8), and the probability distributions (Figure 9). It is worth noting that the sharp, high peaks of I_1/I_3 and I_2/I_3 of the ISM-2 micelle result from the dissociation/association of a few surfactants from/with the micelle.

For further comparison with the results of the 0.215-ns atomistic model MD simulation,[46] Figure 11 focuses on the variations of I_1/I_3 and I_2/I_3 during $t = 9.0-9.2$ ns. The fluctuations of I_1/I_3 and I_2/I_3 for the ISM-2 micelle are quite similar to those for the atomistic model MD simulation.[46] However, I_1/I_3 and I_2/I_3 of the ISM micelle are almost constant within the time scale of 0.2 ns; this result seems unrealistic.

4. Conclusions

Our previously proposed model (ISM) for the simulation of surfactants in aqueous solutions has been revised to improve the representation of surfactant aggregates. In the original ISM, because no water molecules of the solvent are treated explicitly, the effects are incorporated using the solvent-averaged interactions (PMFs) between the surfactant segments in water at infinite dilution, regardless of their surroundings. In the revised model (ISM-2), however, the interactions between the hydrophobic sites of the surfactants are varied depending on the hydrocarbon densities around them. The ISM-2 has been applied to the MD simulations of (i) the single *n*-hexane droplets of different sizes in water and (ii) the single micelle composed of 30 C_{10}TAC cationic surfactants in water where the corresponding simulation with the original ISM was carried out for comparison. The first simulations indicated that the ISM-2 can mimic the *n*-hexane/water interface judging from the density and pressure profiles of *n*-hexane and the interfacial tension. The second simulations demonstrated that the ISM-2 represents the fluidity of the hydrocarbon interior of the micelle successfully, which was confirmed by the atomistic model MD simulation and the NMR measurements; however, the ISM micelle had a solid-like interior of hydrocarbon, which is, of course, unreasonable.

The present ISM-2 simulations satisfactorily represent at least the surfactant aggregates in aqueous solutions with far less computational cost than the atomistic model simulations do, where the water molecules of the solvent as well as the surfactants of interest are treated explicitly. Additionally, the ISM-2 allows us to change the concentration of the surfactants and couterions involved without changing the computational cost because of the implicit treatment of water molecules. Thus, the present model with these advantages will enable us to investigate the self-assembly of surfactants at the molecular level, which requires long-time large-scale simulations.

Finally, we assess the overall nature of our PMF-based ISM from a critical point of view. Unlike the original ISM, the ISM-2 adjusts the PMFs between two hydrocarbon chains depending on the local hydrocarbon density, because the original PMFs are for infinite dilution. Further corrections of the ISM-2 would be required for more accurate simulations. For instance, because the effective concentration of the charged headgroups at the surface of a surfactant micelle is very high, the PMFs between the headgroups might benefit from a similar level of correction. This is also the case for the PMFs between the counterions near the micelle surface and between the charged headgroup and

counterion. Moreover, some level of correction could improve the representation of the liquid−liquid interface between the hydrocarbon oil and implicit water, because the normal pressure profile shown in Figure 5 exhibits a peak at the surface of an oil droplet and this peak is indeed an artifact of the simulation with the ISM-2. These corrections of the ISM family will be our future study.

Acknowledgment. This work was partly supported by the Grants-in-Aid (no. 15206085/16760606) for Scientific Research from the Ministry of Education, Culture, Sports, Science and Technology in Japan. S.M. thanks Hosokawa Powder Technology Foundation, for partly supporting his study in 2004. Visualization of the simulation data was performed at the Academic Center for Computing and Media Studies, Kyoto University.

References and Notes

(1) Holmberg, K.; Jönsson, B.; Kronberg, B.; Lindman, B. *Surfactants and Polymers in Aqueous Solution*, 2nd ed.; Wiley: Chichester, U.K., 2003.
(2) Larson, R. G. *The Structure and Rheology of Complex Fluids*; Oxford University Press: New York, 1999.
(3) Meier, W. *Curr. Opin. Colloid Interface Sci.* **1999**, *4*, 6.
(4) Miller, S. A.; Ding, J. H.; Gin, D. L. *Curr. Opin. Colloid Interface Sci.* **1999**, *4*, 338.
(5) (a) Hentze, H.-P.; Antonietti, M. *Curr. Opin. Solid State Mater. Sci.* **2001**, *5*, 343. (b) Hentze, H.-P.; Antonietti, M. *Rev. Mol. Biotechnol.* **2002**, *90*, 27. (c) Hentze, H.-P.; Kaler, E. W. *Curr. Opin. Colloid Interface Sci.* **2003**, *8*, 164.
(6) Mueller, A.; O'Brien, D. F. *Chem. Rev.* **2002**, *102*, 727.
(7) Holmberg, K. *J. Colloid Interface Sci.* **2004**, *274*, 355.
(8) Allen, M. P.; Tildesley, D. J. *Computer Simulation of Liquids*; Clarendon Press: Oxford, U.K., 1987.
(9) Frenkel, D.; Smit, B. *Understanding Molecular Simulation: From Algorithms to Applications*, 2nd ed.; Academic Press: San Diego, 2002.
(10) Rapaport, D. C. *The Art of Molecular Dynamics Simulation*, 2nd ed.; Cambridge University Press: Cambridge, U.K., 2004.
(11) Klein, M. L. *J. Chem. Soc., Faraday Trans.* **1992**, *88*, 1701.
(12) Smit, B. In *Computer Simulation in Chemical Physics*; Allen, M. P., Tildesley, D. J., Eds.; NATO Advanced Study Institute Series C; Kluwer: Dordrecht, The Netherlands, 1993; Vol. 397, Chapter 12.
(13) Pastor, R. W. *Curr. Opin. Struct. Biol.* **1994**, *4*, 486.
(14) Esselink, K.; Hilbers, P. A. J.; Karaborni, S.; Siepmann, J. I.; Smit, B. *Mol. Simul.* **1995**, *14*, 259.
(15) Karaborni, S.; Smit, B. *Curr. Opin. Colloid Interface Sci.* **1996**, *1*, 411.
(16) Larson, R. G. *Curr. Opin. Colloid Interface Sci.* **1997**, *2*, 361.
(17) Jakobsson, E. *Trends Biochem. Sci.* **1997**, *22*, 339.
(18) Bandyopadhyay, S.; Tarek, M.; Klein, M. L. *Curr. Opin. Colloid Interface Sci.* **1998**, *3*, 242.
(19) Shelley, J. C.; Shelley, M. Y. *Curr. Opin. Colloid Interface Sci.* **2000**, *5*, 101.
(20) Feller, S. E. *Curr. Opin. Colloid Interface Sci.* **2000**, *5*, 217.
(21) Forrest, L. R.; Sansom, M. S. P. *Curr. Opin. Struct. Biol.* **2000**, *10*, 174.
(22) Schmid, F. In *Computational Methods in Surface and Colloid Science*; Borówko, M., Ed.; Surfactant Science Series 89; Marcel Dekker: New York, 2000; Chapter 13.
(23) Saiz, L.; Bandyopadhyay, S.; Klein, M. L. *Biosci. Rep.* **2002**, *22*, 151.
(24) Roux, B.; Simonson, T. *Biophys. Chem.* **1999**, *78*, 1.
(25) Shinto, H.; Morisada, S.; Miyahara, M.; Higashitani, K. *Langmuir* **2004**, *20*, 2017.
(26) (a) Shinto, H.; Morisada, S.; Miyahara, M.; Higashitani, K. *J. Chem. Eng. Jpn.* **2003**, *36*, 57. (b) Shinto, H.; Morisada, S.; Higashitani, K. *J. Chem. Eng. Jpn.* **2004**, *37*, 1345. (c) Shinto, H.; Morisada, S.; Higashitani, K. *J. Chem. Eng. Jpn.*, to be published.
(27) The Chemical Society of Japan. *Kagaku-binran Kiso-hen II*, 4th ed.; Maruzen: Tokyo, Japan, 1993.
(28) Ryckaert, J.-P.; Bellemans, A. *Faraday Discuss. Chem. Soc.* **1978**, *66*, 95.
(29) Higashitani, K.; Iimura, K.; Sanda, H. *Chem. Eng. Sci.*, **2001**, *56*, 2927.
(30) Solomons, T. W. G. *Organic Chemistry*, 6th ed.; Wiley: New York, 1996.
(31) Ozeki, S.; Ikeda, S. *Bull. Chem. Soc. Jpn.* **1981**, *54*, 552.
(32) Imae, T.; Ikeda, S. *J. Phys. Chem.* **1986**, *90*, 5216.
(33) Reiss-Husson, F.; Luzzati, V. *J. Phys. Chem.* **1964**, *68*, 3504.
(34) Bacaloglu, R.; Blaskó, A.; Bunton, C. A.; Cerichelli, G.; Ortega, F. *J. Phys. Chem.* **1990**, *94*, 5062.
(35) Klevens, H. B. *J. Am. Oil Chem. Soc.* **1953**, *30*, 74.
(36) Irving, J. H.; Kirkwood, J. G. *J. Chem. Phys.* **1950**, *18*, 817.
(37) Thompson, S. M.; Gubbins, K. E.; Walton, J. P. R. B.; Chantry, R. A. R.; Rowlinson, J. S. *J. Chem. Phys.* **1984**, *81*, 530.
(38) Mitrinović, D. M.; Tikhonov, A. M.; Li, M.; Huang, Z.; Schlossman, M. L. *Phys. Rev. Lett.* **2000**, *85*, 582.
(39) Rivera, J. L.; McCabe, C.; Cummings, P. T.; *Phys. Rev. E* **2003**, *67*, 011603.
(40) Maruyama, S.; Matsumoto, S.; Ogita, A. *Therm. Sci. Eng.* **1994**, *2*, 1.
(41) Zakharov, V. V.; Brodskaya, E. N.; Laaksonen, A. *Mol. Phys.* **1998**, *95*, 203.
(42) Zakharov, V. V.; Brodskaya, E. N.; Laaksonen, A. *J. Chem. Phys.* **1998**, *109*, 9487.
(43) Zeppieri, S.; Rodríguez, J.; López de Ramos, A. L. *J. Chem. Eng. Data* **2001**, *46*, 1086.
(44) Nijmeijer, M. J. P.; Bruin, C.; van Woerkom, A. B.; Bakker, A. F.; van Leeuwen, J. M. J.; *J. Chem. Phys.* **1992**, *96*, 565.
(45) Reid, R. C.; Prausnitz, J. M.; Poling, B. E.; *The Properties of Gases and Liquids*, 4th ed.; McGraw-Hill: New York, 1987.
(46) Böcker, J.; Brickmann, J.; Bopp, P. *J. Phys. Chem.* **1994**, *98*, 712.
(47) Stilbs, P.; Walderhaug, H.; Lindman, B. *J. Phys. Chem.* **1983**, *87*, 4762.